Spatial and Temporal Analysis of the relation of urban heat island with vegetation cover in Tehran

Alireza Sadeghinia[1,*], Bohloul Alijani[2]

1- Department of Geography, Kharazmi University, Tehran, Iran.
2- Professor of climatology and Director of Center of Excellence for Spatial Analysis of Environmental Hazards, Kharazmi University, Tehran, Iran.

* Corresponding Author: Alirezasadeghinia@gmail.com

Received: 08 July 2015 / Accepted: 18 October 2015 / Published online: 29 October 2015

Abstract

The rapid change of land use and land cover in the Metropolitan area of Tehran has influenced the distribution pattern of land surface temperature (LST). In this study, a spatial autocorrelation analysis is adopted to process the spatial-temporal changes of LST and Normalized Difference Vegetation Index (NDVI) in Tehran during the period of 1987 to 2010. Global spatial autocorrelation analysis revealed that global Moran's I of LST has increased while that of NDVI has decreased with time. While the newly hot clusters of LST were appeared in west and southwest of Tehran, the spatial extents of the old hot clusters have been increased. The Local Indicators of Spatial Association (LISA) analysis confirmed the intensifying and expansion of the hot clusters and weakening of the cold clusters of LST. The spatial pattern of LST and UHI expanded toward west and southwest of Tehran and UHI effect was intensified. Based on LISA analysis, the occurrence of increasing trend of HH cluster of LST is related to the decrease of HH cluster of NDVI in Tehran. Accompanying with decreasing of vegetation cover, green cover cooling effect also decreased, and consequently, UHI effect was intensified from 1987 to 2010. The results demonstrate the usefulness of spatial autocorrelation technique for analysis of spatial-temporal changes of UHI and green cover in urban areas. Ordinary Least Squares regression (OLS) and Geographically Weighted Regression (GWR) were used to investigate the relationships between LST and NDVI. The results indicate that the performance of the GWR model is significantly better than OLS.

Keywords: Urban heat island; Green cover; Spatial-temporal changes of temperature; The global and local spatial autocorrelation; The geographically weighted regression.

1- Introduction

Urbanization changes the land cover types in urban areas and results in distinguished climatic conditions termed the "Urban climate". Urban climates are distinguished from surrounding rural climates by differences of air temperature, humidity, wind speed and direction and amount of precipitation (Rose and Devadas, 2009). Urbanization modifications generally lead to a thermal climate that is warmer than the surrounding non-urban areas. This phenomenon is called the urban heat island (UHI) (Vooget and Oke, 2003). The UHI effect results in a climate of about 3.5-4.5°C warmer than surrounding rural areas and is expected to increase by approximately 1°C per decade. The temperature differences between urban and surrounding rural areas can reach up to 10° C for large urban agglomerations (Voogt, 2002).

Adaptation to rising temperatures by increasing air condition can also further increase UHI effects. For instance, massive air conditioning has been shown to increase UHI effects up to 1°C (Hallegatte *et al*., 2008). There is also recent evidence that local precipitation rates may be affected by urbanization. For example, the analysis of precipitation in Phoenix, Arizona, showed that the post-urbanization precipitation is significantly higher than the pre-urbanization amount (Ruth and Gasper, 2008).

The traditional method for studying UHI effect has long been based on the observed temperature at the meteorological stations or thermometers boarded on moving vehicles (Streutker, 2002; Weng, 2004), which might not fully represent the areal variations of urban temperatures due to their scarcity and uneven distribution. But since the 1960s, Remote Sensing technology has been widely used to measure land surface temperature (LST) (Liu and Zhang, 2011) with a very higher spatial resolution compared to the traditional method. At the beginning, UHI was studied with NOAA AVHRR thermal data (Balling and Brazell 1988; Gallo *et al*. 1993; Gallo and Owen 1988; Streutker 2002) but later, the utilization of thermal infrared data of TM, ETM + and ASTER improved the precision of the studies (Weng 2001; Weng *et al*. 2006; Amiri *et al*. 2009; Flahatlar *et al*. 2011). For example, Amiri *et al*. (2009) explored spatial–temporal dynamics of land surface temperature in relation to fractional vegetation cover and land use/cover in Tabriz urban area, Iran. They used multi-temporal images of Landsat 4, 5 TM and 7 ETM+ sensors to examine the relationship between LST and land use/cover (LULC). Most of the studies found that the multi-temporal satellite data are very effective in studying urban vegetation and temperature changes (Dai *et al*., 2010; Mo *et al*., 2011; Xu *et al*., 2011). According to some studies (Xu 2004; Zhang *et al*., 2007; Du *et al*., 2009; Sun *et al*., 2010; Xu *et al*., 2011; Chen *et al*., 2002; Li *et al*., 2009; Dai *et al*., 2010) the UHI effect is increasing through the time. For instance, Zhang *et al*. (2007) analyzed the areal extension of UHI in the estuarine area of Pearl River (China) from 1990 to 2000 by Landsat TM/ETM+ data and indicated that the area has increased about 250 square kilometers during the study period. Li *et al*. (2009) used the integrated GIS/RS approach and spatial analysis methods such as spatial autocorrelation, semivariance, and fractal analysis to demonstrate the increasing trend of the magnitude and spatial extent of UHI in the Shanghai metropolitan area during the 1997-2004.

The urban area of Tehran (Fig. 1), with more than 8 million populations is located on the southern foothills of Alborz Mountains at an average elevation of 1600 meters. Due to rapid immigration of population, increasing energy consumption and resultant changes in land use and land cover, uncontrolled urbanization and industrialization have led to an overall environmental degradation in this region. Large scale urban constructions and industrial enterprises increased the city heat capacity and temperature, resulting in high temperature difference between urban and surrounding areas and thus more effective UHI. Some researchers (Akbari, 2000; Jangi, 2004; Namdari, 2009) have studied the UHI in Tehran. For example based on the land use/cover interpretation of a LANDSAT image of August 9, 2002, Namdeari (2009) has stated that the highest temperatures were shown in the areas of most populated, transportation terminals and airport, and in barren lands. The main point is that none of the previous researches have given a comprehensive image and understanding of the temperature variation of Tehran and the UHI. For this reason, the main objective of this research is to study the spatial and temporal changes of UHI in Tehran urban area in relation to changes of green cover.

2- Materials and Methods

To explore the spatial-temporal changes of urban thermal environment of Tehran, the first LST is retrieved from multi- temporal Landsat TM thermal channel data (2 images) by using mono-window algorithm. Then, Normalized Difference Vegetation Index (NDVI) was computed for all images from visible (0.63–0.69 mm) and near-infrared (0.76–0.90 mm) data of the Landsat TM. Based on the data, global and local spatial autocorrelation analysis was adopted to reveal the characteristics of spatial heterogeneity and temporal change of LST and NDVI at different scales and periods. Finally, Ordinary Least Squares regression (OLS) and Geographically Weighted Regression (GWR) were used to investigate the relationship between LST and NDVI. More details about the data and the analysis are described in the following sections.

2.1- Image and pre-processing

This research used Landsat TM5 (launched in 1984) 10.4-12.5 μm thermal band data with a spatial resolution of 120 m. Two scenes of Landsat TM image for days 23 July 1987 and 22 July 2010, were acquired. The data source was the USGS, which had corrected the radiometric and geometrical distortions. The TM image was rectified to UTM coordinate system, and was resampled using the nearest neighbor algorithm with a pixel size of 30 by 30 m for all bands. The resultant RMSE was found to be less than 0.5 pixels. From the available TM data, two scenes without visible clouds in the area of interest were selected for further processing and LST calculations. Furthermore, the NDVI was calculated from the Landsat bands 3 (RED) and 4 (NIR) of the same scenes. To gain the final images of LST and NDVI in Tehran city, the resultant images were clipped based on urban area boundary file. The air temperature and moisture data were obtained from four weather stations (Mehrabad, Chitgar, Geophysique, Dooshantappeh and Aghdasieh) as an auxiliary data to use for retrieving LST from the thermal remote sensing images. The data pre-processing and other analyses were performed using ERDAS Imagine 9.2 and ArcGIS 10 software.

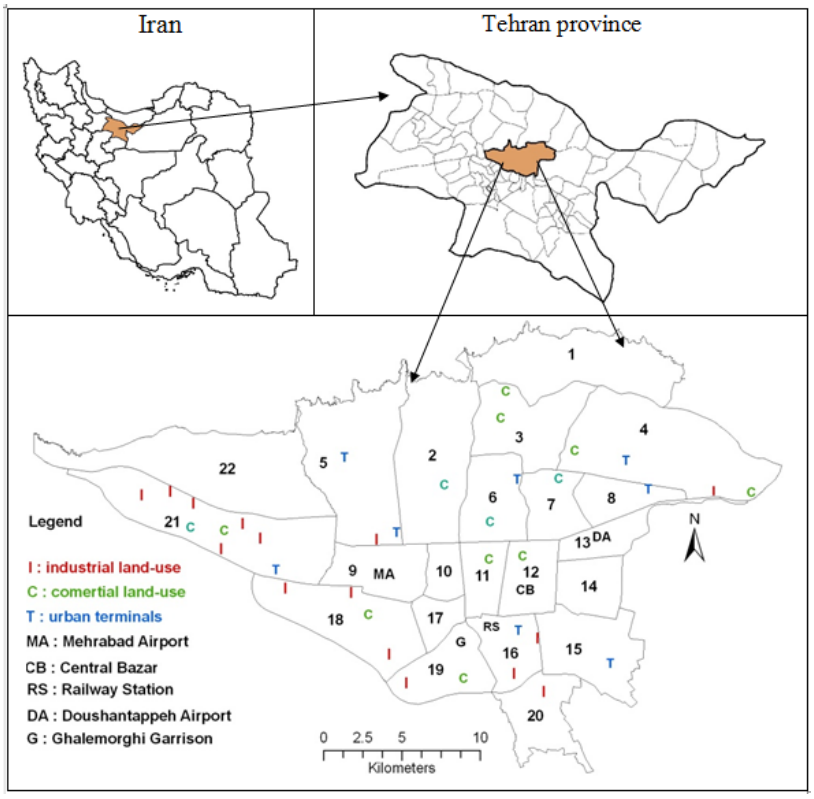

Figure 1) The study area (The Metropolitan of Tehran). The most effective land-use types for the establishment of UHI are presented on the map by their initials. The numbers represent the 22 districts of Tehran.

2.2- Retrieving land surface temperature

The thermal band data of Landsat TM (TM6) is highly suitable for analyzing the spatial patterns of the Earth's heat flux variation and surface temperature. In this study, the mono-window algorithm is used for Landsat TM 6. In 2001, Qin *et al*. proposed the mono-window algorithm (Figure 3) for retrieving LST from Landsat TM 6 data (Qin *et al*, 2001). Based on thermal radiance transfer equation, the mono-window algorithm only requires three parameters— emissivity, transmittance and effective mean atmospheric temperature— to retrieve LST from Landsat TM 6 through the following steps:

1) Converting the digital number (DN) into brightness temperature: The digital numbers (DN) of band 6 were converted to a sensor radiance using equation (1) (Chander and Markham, 2003):

$$[L_\lambda = \left[\frac{(L_{max}-L_{min})}{(Qcal_{max}-Qcal_{min})}\right] Qcal + L_{min}] \quad (1)$$

where L_{min} and L_{max} are spectral radiance for band 6 at DN 0 and DN 255 respectively; Qcal=DN, $Qcal_{min}$=0 , $Qcal_{max}$=255.

The above spectral radiance values from the TM thermal band were transformed to brightness temperature according to equation (2):

$$[T_6 = \frac{K_2}{\left\{L_n\left[\frac{K_1}{L_\lambda}+1\right]\right\}}] \quad (2)$$

Where, T6 is at-satellite brightness temperature in kelvin; K1 and K2 are pre-launch calibration constants. For TM images, K_1=607.76 W/m^2/sr/um, K_2=1260.56K. L_λ:Spectral radiance in (W/m2/sr/um).

2) Calculation of land surface emissivity: The emissivity can be estimated by utilizing NDVI (Van De Griend and Owe. 2003) (Table 1). In order to calculate the NDVI, Equation (3) can be used as:

$$[NDVI = \frac{NIR-R}{NIR+R} \quad (3)$$

Then, a complete land surface emissivity estimation method proposed by Zhang *et al*. (2006) was utilized to calculate emissivity for each pixel.

Table 1) Estimation of emissivity by using NDVI (Zhang et al., 2006).

NDVI	Land surface emissivity (ε_i)
NDVI< -0.185	0.995
-0.185≤ NDVI≤ 0.157	0.97
0.157≤ NDVI ≤ 0.727	1.0094 + 0.047 Ln. (NDVI)
NDVI > 0.727	0.99

3) Calculation of atmospheric transmittance: Actually, the atmospheric transmittance can be estimated by using water vapor (Liu and Zhang, 2010). In order to calculate the water vapor, Equation 4 is used (Li *et al*., 2006).

$$[W_i = 0.0981 \times \left\{10 \times 0.6108 \times \exp\left[\frac{17.27\times(T_0-273.15)}{237.3+(T_0-273.15)}\right] \times RH\right\} + 0.1697] \quad (4)$$

Where, w_i is the water vapor content (g/cm^2); T^0 is the near-surface air temperature in K; and RH represents the relative humidity. The data for water vapor content, near-surface air temperature and relative humidity of Tehran meteorological stations were used for the same dates Landsat TM images (date 23 July 1987 and 22 July 2010). Then, Equations of Table 2 were applied to calculate the atmospheric transmittance of Landsat TM 6 (Qin *et al*., 2001).

Table 2) Estimation of atmospheric transmittance (Qin et al., 2001).

Profiles	water vapor (w) (g/cm^2)	Transmittance estimation equation (τ_i)
High air temperature	0.4 - 1.6	0.974290 - 0.08007w
	1.6 - 3.0	1.031412 - 0.11536w
Low air temperature	0.4 - 1.6	0.982007 - 0.09611w
	1.6 - 3.0	1.053710 - 0.14142w

In this table, τ_i is the atmospheric transmittance of Landsat TM 6 and w represents the water vapor content which was calculated using Equation (4).

4) The atmospheric effective mean temperature was calculated using the equation (5), because it is adequate according to the location of Tehran in summer (Qin *et al*., 2001).

$$[Ta = 16.0110 + 0.92621 \times T_o] \quad (5)$$

Where, T_o is the near-surface air temperature in K.

5) Final retrieving of LST: After the calculation of the values of the three variables of emissivity, transmittance and effective mean atmospheric temperature, the mono-window algorithm was processed:

$$[T_s = \{a(1 - C - D)[b(1 - C - D) + C + D]T_i - DT_a\}/C] \quad (6)$$

$$C = \varepsilon_i \times \tau_i \ , \ D = (1 - \tau_i)[1 + (\varepsilon_i) \times \tau_i]$$

Where T_s is the LST (k), two constants (a and b) are 67.355351 and 0.458606, respectively. T_i is the at-sensor brightness temperature (k), Ta represents the effective mean atmospheric temperature that is calculated using equation (5). The ε_i is the emissivity, which is classified and computed by NDVI (Table 1), τi is the transmittance given in the Table 2.

2.3- Detection of spatial and temporal changes of LST and Vegetation cover

The spatial autocorrelation provides information on the spatial structure of the variables, which is a powerful approach for the analysis of spatial patterning in geography, and such methods have been successfully applied in climatological researches (Li *et al*. 2009; Su *et al*. 2011; Dai *et al*. 2010). Moran's I index is the most used index to assess the global level of spatial autocorrelation (Anselin, 1995). Given a set of features and an associated attribute, global spatial autocorrelation analysis evaluates whether the pattern is clustered, dispersed, or random; the local spatial autocorrelation analysis determines the location and intensity of the clustered pattern. In this study, global and local spatial autocorrelations were used to quantify the spatial and temporal changes of LST and NDVI (green cover) in Tehran area from 1987 to 2010. The Moran's Global I statistic was used to measure the global spatial autocorrelation of the LST and NDVI data (Dai *et al*., 2010):

$$[I = \frac{N}{S_o} \times \frac{\sum_{i=1}^{N}\sum_{j=1}^{N} w_{ij}(x_i - \bar{x})(x_j - \bar{x})}{\sum_{j=1}^{N}(x_i - \bar{x})_i^2}] \quad (7)$$

where, N is the total number of cells, Xi and Xj are the values of the observed variable at cells i and j, $\overline{X}$ is the mean of all Xi and Xj , $\bar{x} = \frac{1}{N}\sum_{i=1}^{N} x_i$, $s_o = \sum_{i=1}^{N}\sum_{j=1}^{N} w_{ij}$, Wij, the weights representing proximity relationships between cell i and j, indicating the influence extent of spatial structure dependence, and determined according to adjacent relationship in this paper. Usually, the Moran's I should be standardized to z for judging the positive or negative correlation and statistical test of results. In general, the value of Moran's I vary between -1.0 and +1.0. A higher positive I implies that the values in neighboring sites tend to cluster together. Whereas a lower negative I implies that high and low values are interspersed. Moreover, the value of I near zero reveals that the data are randomly distributed without spatial autocorrelation (Cliff and Ord, 1981; Legendre and Legendre, 1998).

The Global Moran's I only indicates overall clustering extent but cannot be used to detect spatial association pattern in different locations (Dai *et al*., 2010). To further reveal the spatial autocorrelation of LST (NDVI) in the

neighborhoods and visualize the spatial pattern of local differences, the Local Indicators of Spatial Association (LISA) were used. LISA analysis include Local Moran's I and Local Geary's C. The local Moran's I is used to evaluate the local spatial association and difference between each cell and its surrounding cells. Local Moran's I is the disintegration form of Global Moran's I. For a given spatial cell i, the value of Local Moran's I is computed as (Anselin, 1995):

$$[I_i = x_i \sum_{i=1,j\neq i}^{N} w_{ij} x_j] \quad (8)$$

Where, N is the number of cells, X_i and X_j are the standardized observed value of cell i and j, and W_{ij} is the standardized spatial weighting value ($\sum_j w_{ij}$ =1). Similar to the significance test of Global Moran's I, the results of the Local Moran's I can be tested by means of Z-Score. Given a certain significance level, if the Ii value is significantly positive, then the cell Ii has value similar to neighboring cells' values, and a spatial cluster of similar LST (NDVI) values surrounds the cell i, meaning a spatial positive correlation. A high positive I_i value demonstrates a strong clustering extent. On the other hand, if the I_i value is significantly negative, then the cell I_i has a very different LST (NDVI) value than its neighbors, indicating a spatial negative correlation. With the local Moran's I statistics analysis, three types of local spatial autocorrelation were distinguished. The clustered type occurs when high values surrounded by high values (High-high), or low values surrounded by low values (Low-low). The pattern is dispersed, if high values surrounded by low values (High-low) and low values surrounded by high values (Low-high). The third type is the spatial randomness with no distinguished spatial behavior (Huo *et al*., 2012). Among these spatial patterns, HHs are called hot spots and LLs are called cold spots. According to the spatial distribution of HHs and LLs, the location and spatial variation of urban heat island and urban cold spots were defined, respectively. Their temporal variations were achieved by studying their annual frequencies through the study period.

2.4- Statistical analysis of the LST-NDVI relationship

The Ordinary Least Square regression (OLS) and Geographically Weighted Regression (GWR) models were used to investigate the relationships between LST and NDVI. OLS is well known and has been used in the past, but due to the lack of space factor, does not give higher accuracy. As a global spatial model, the OLS does not have a satisfactory estimating power for the relationship between dependent and explanatory variables. But the GWR model allows the regression coefficient to take different values for each prediction point. In other words, the regression coefficients are not constant over the geographical space (Bostan *et al*., 2012). Thus the GWR technique extends the conventional global regression by adding a geographical location parameter, and is written as (Gao *et al*., 2012):

$$[y_i = \beta_0(\mu_i, v_i) + \sum_{k=1}^{p} \beta_k(\mu_i, v_i)\, x_{ik} + \varepsilon_i \ , i = 1,2] \quad (9)$$

Where, y_i is the observed value of the dependent variable at location i, x_{ik} is the observation of the explanatory variable at location (μ_i, v_i) , $\beta_0(\mu_i, v_i)$ represents the intercept at location i, $\beta_k(\mu_i, v_i)$ represents the local parameter estimate for explanatory variable x_k at location i, and ε_i (i = 1, 2,…,n) is the random error term at point i. To estimate the parameters in Eq. (9), an observation is weighted according to its proximity to a specific point i, Therefore, the weighting of an observation in the analysis is not constant, but a function of geographical location. The parameters in Eq. (9) may be estimated by solving the following matrix equation (Gao *et al*., 2012):

$$[\hat{\beta}(\mu, v) = (X^T W(\mu, v) X)^{-1} X^T W(\mu, v) Y] \quad (10)$$

where, $\hat{\beta}(\mu, v)$ represents the unbiased estimates of β, and $W(\mu, v)$ is the weighting matrix, whose role is to ensure that observations nearer

to the specific location have larger weight. In this study we used the following Gaussian weighting kernel function form (Fotheringham *et al*., 2002; Li *et al*., 2012):

$$[w_{ij} = \exp\left(\frac{d_{ij}^2}{b^2}\right)] \quad (11)$$

where, d_{ij} is the Euclidean distance between regression point i and neighboring observation j, and b represents a basal width of the kernel function, called bandwidth (Li *et al*., 2012). The comparison of the regression models can be achieved by several diagnostic statistics, such as: AIC (Akaike Information Criterion), R2, adjusted R2 and Sigma (the square root of the normalized residual sum of squares). All of these diagnostic statistics were used to compare the models. In this research, GWR and OLR analysis was carried out using ArcGIS 9.3. The TM image of the day 2010/8/7 was selected to carry out this analysis. Initially, the NDVI raster layer resampled to 120 m spatial resolution to make similar spatial resolutions of both LST and NDVI layers, and then, all layers were converted to vector format.

3- Results and Discussion

3.1- Spatial-temporal changes of LST and NDVI

3.1.1- Global Spatial Autocorrelation

To explore the spatial autocorrelation of the LST in the study area at different scales, the resultant LST images are resampled to the spatial resolution of 360, 720 and 960 m. Table 3 shows the values of Global Moran's I of the LST images at different levels of spatial resolution. The values of Global Moran's I of all images are significantly positive, which indicates that the LST in Tehran has a characteristic of spatial aggregation with significant spatial positive correlation. Table 3 shows the z scores of the global spatial autocorrelation analysis, which have high global autocorrelation coefficients. These coefficients are much higher than the threshold value of 2.54 (with 0.01 level of the significance); this also confirms that the LST in Tehran has strong spatial autocorrelation and the hypothesis of randomness is rejected. Thus, the LST of Tehran is clustered such that the higher LST values are surrounded by higher LST neighbors and lower LST values by lower LST neighbors. The value of Global Moran's I decreases as the spatial scale increases, the Global Moran's I reaches 0.86, 0.72, 0.51 and 0.46 at the scales of 120, 360, 720 and 960 m in 1987. Also, it reaches 0.877, 0.778, 0.62 and 0.593 at the scales of 120, 360, 720 and 960m in 2010 (Table 3). It can be concluded that the amount of similarity of LST values in Tehran is greater at small scales than the large spatial scales. In other words, at the larger spatial scales (such as 720 and 960 m) the small hot and cold clusters disappear and only the big clusters remain. Consequently, we can obtain more details in relation to UHI at the small spatial scales (such as 120m) in the study area .

*Table 3.Global Moran's I values in different levels of spatial resolution for LST (*Significant at 0.01 level).*

Date of images	Spatial resolution	Global Moran's I	Z	Date of image	Spatial resolution	Global Moran's I	Z
	120	0.86 *	253		120	0.877 *	254
1987/7/23	360	0.72 *	95.1	**2010/7/22**	360	0.778 *	102
	720	0.51 *	33.2		720	0.62 *	40.4
	960	0.46 *	16.1		960	0.593 *	20

Table 3 shows the temporal changes of the distribution of LST in the study area. The global spatial autocorrelation of LST indicates an increasing trend through the study period. It was 0.86 in 1987 for 120 m resolution but increased to 0.877 in 2010. Also, it increased from 0.46 to 0.593 for 960 m resolution. The increasing trend of global spatial correlation has two possible implications. On one hand, the increase could be due to the LST of pixels in each cluster

becoming more similar in Tehran. On the other hand, it might result from the emergence of newly formed clusters. The Moran's global I does not help us distinguish between these possibilities. As a result we calculated the local spatial autocorrelation analysis to disclose these differences.

In order to explore spatial- temporal changes of the distribution of green cover in Tehran and compare it to LST, Moran's I was also calculated for NDVI. Table 4 shows the values of Global Moran's I of the NDVI at spatial scales of 30 and 120m. Similar to those of LST, the values of Global Moran's I of all NDVI images are significantly positive (statistically significant at 0.01 level), which indicate that a clustered pattern exists for NDVI as well. According to Table 4, the global spatial autocorrelation of NDVI has decreased during the 1987- 2010 period. For example, it was 0.85 in 1987 for 30 m resolution but decreased to 0.81 in 2010. It can be guessed that many of the hot or cold clusters of NDVI were diminished or fragmentized during the study period. Consequently, the increasing trend of global spatial autocorrelation of LST could be related to decreasing trend of global spatial autocorrelation of NDVI values. As it is mentioned above, to obtain more assurance, the local spatial autocorrelation index was calculated.

*Table 4) Global Moran's I values in different levels of spatial resolution for NDVI (*Significant at 0.01 level).*

Date of images	Spatial resolution	Global Moran's I	Z	Date of image	Spatial resolution	Global Moran's I	Z
	30	0.85 *	1651		30	0.81 *	1612
1987/7/23	120	0.61 *	122.2	**2010/7/22**	120	0.51 *	159

3.1.2- Local Indicators of Spatial Association (LISA)

The LISA maps can further detect the locations of the interesting spatial patterns for both LST and NDVI variables. The results of the LISA statistics for LST are shown in Fig. 2. According to Figs. 2a and 2b the hot clusters (HH clusters) are distributed mainly on the west and southwest of Tehran, especially over the Mehrabad airport in district 9 and highly industrialized zone and bare lands of districts 22, 21, 18, 9 and 5. Undoubtedly, the main center of UHI is continuously located over the west and southwest of Tehran during the study period, with the Mehrabad airport being the hottest spot. The other hot spots are dispersed all over the city, especially in the old downtown and central Bazaar, Dooshantappeh Airport, Ghale-Morghi, Railway Station, bus terminals, big silo, factories and etc. (see Fig. 1). The mostly vegetated northeast region of Tehran is strongly occupied by the LL clusters of LST (Figs. 2a and 2b). Therefore, the cold spot of Tehran is situated in the north of Tehran over Shemiranat and considerable portion of districts 2, 3 and 4. The other LL clusters correspond mostly to the green areas and urban parks.

Comparison of the LISA cluster maps for the period 1987-2010 shows that the spatial distribution of hot spots have shifted westward during the study period (Figs. 2a and 2b). Despite the weakening or disappearing of some hot spots in districts 1, 2, 3 and 5; the most important spatial changes have been occurred in the parts of Western and South-West of Tehran. The hot spots that situated in district 22 have been moved to the West and strengthened. In addition, the new hot clusters have appeared in west and south west (i.e. in districts 9, 18, 19 and 21). In contrast, the green space and cover has been diminished in the west of the city.

On the contrary, some of LL clusters disappeared or were fragmented during the

study period. For example, some of the LL clusters of the southern and western parts of the city (districts 19, 18, 21 and 22) diminished or were fragmented in 2010.

Based on the appearance and expansion of the HH clusters and gradual decrease of LL clusters in the west and southwest of Tehran (District 9, 18, 19, 21 and 22), the area and intensity of Tehran UHI gradually spread and strengthened at the expense of cold spots of the city. There are probably many reasons for expanding of UHI effect in Tehran. First, the expansion direction of UHI is accordant with the spatial expansion of industrial, transport and commercial land use in the west, southwest and south of Tehran (districts 22, 21, 18 and 19). Therefore, it can be concluded that the expansion of these infrastructures have played the most important role in intensification of the UHI effect in west and southwest of Tehran. These land use types were covered by dark materials (such as asphalt, concrete, etc.) and metallic roofs (galvanized or aluminum materials) that have a low reflectivity, so they absorb and store solar energy instead of reflecting them. This warms the environment. Second, the dispersed bare land spots of the area forms the hottest places during the hot seasons of the year. Third, the large quantities of vegetation cover have been cut and disappeared overall the city (especially in the districts 18, 19, 21 and 22).

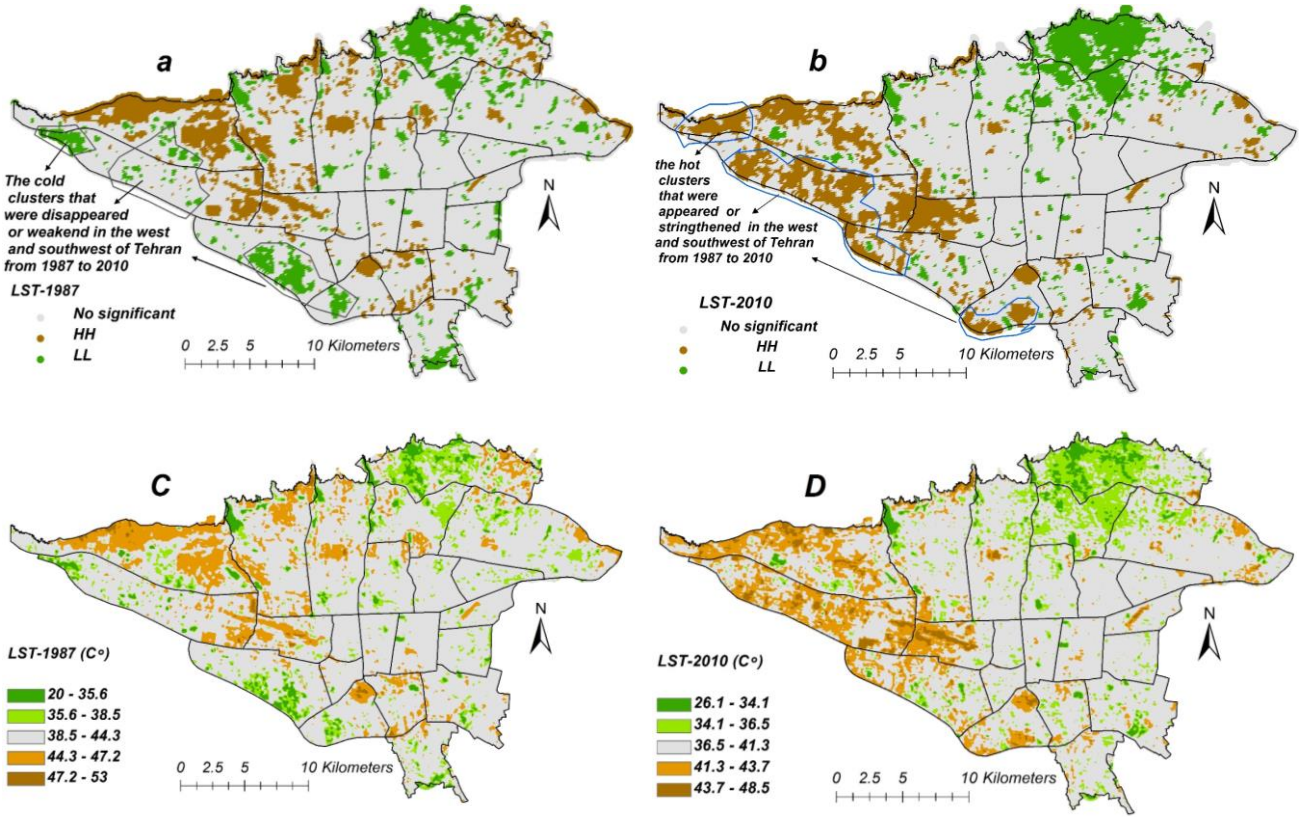

Figure 2) The spatial pattern of LISA clusters in 1987/7/23 (a) and 2010/7/22 (b). The LST maps of these images are shown in (c) (1987/7/23) and (d) (2010/7/22)

The spatial distribution of NDVI clusters are shown in Fig. 3. In 1987, the HH clusters were locally concentrated in the north (district 1, 2, 3 and 4), southwest (district 18) and west of the study area (districts 21, 22 and 5) (Fig. 3a). But in 2010, the HH clusters have been decreased considerably, especially in the north, west (districts 9, 21 and 22), and southwest of Tehran (districts 18, 19) (Fig. 3b). This decreasing trend of green space HHs increased the HH clusters of LST as is seen in Fig. 2.

To clarify this spatial correlation, the LISA statistics were calculated and presented in Tables 5 and 6. According to these tables the number of HH clusters of LST has increased while that of NDVI has decreased. That is, as the green space coverage decreased, the extent and intensity of hot spots increased. At the same time a number of cold spots were decreased. Thus during the study period the whole city has gone under warming process. And the overall temperature of the city has increased. Another indication for this overall warming trend of the city is the absence of HL or LH spots of temperature through the study period. In other words, the warming trend of the city is relatively homogenous over the city. But on the other hand the spatial change of the NDVI clusters is not homogenous over the city.

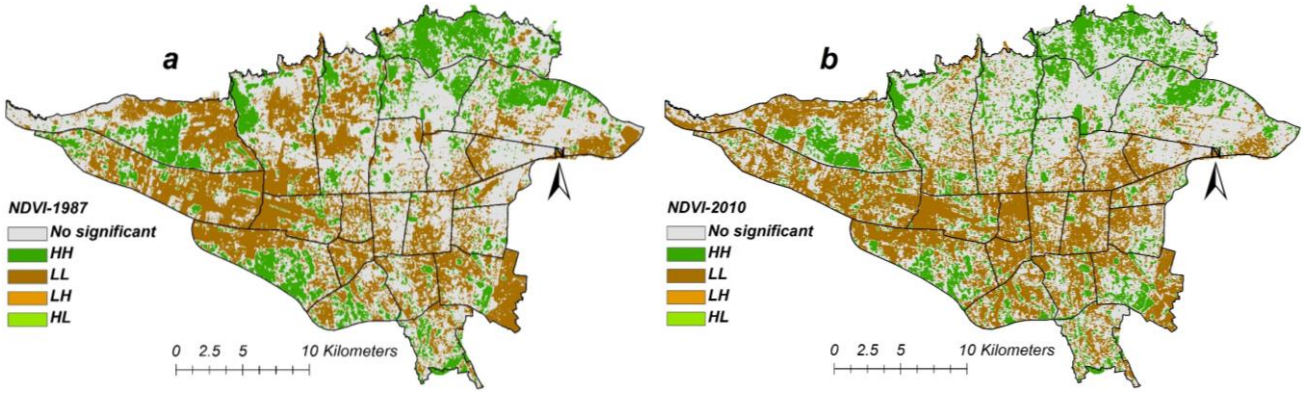

Figure 3a) The LISA clusters map of NDVI in 1987/7/23 and b) 2010/7/22.

Table 5) Frequency of local spatial clusters of the LST in 120 meters spatial resolution.

Date of images	No significant	High-High	Low-Low	Low-High	High-Low
1987/7/23	31442	6098	5060	0	0
2010/7/22	31419	6466	4715	0	0

Table 6) Local spatial autocorrelation characteristics of NDVI in 120 meters spatial resolution.

	Frequency of local spatial clusters				
Date of images	No significant	High-High	Low-Low	Low-High	High-Low
1987/7/23	37361	4829	343	30	37
2010/7/22	37876	3794	509	61	120

3.2- The LST-NDVI relationship

In order to compare the green cover and urban heat island effects, statistical analysis of the LST-NDVI relationship is carried out. The correlation coefficient of LST and NDVI is -0.54 being significant at 0.05 level. It indicates that the expansion of the green space can weaken the urban heat island effect. Table 7 shows the results of GWR and OLR models. Based on diagnostic statistics of Table 7, the GWR model is better than the OLS model, because the GWR has the higher R2, lower AIC, and lower Sigma values. This better performance of the GWR model is due to the fact that this model uses a geographical parameter which is very good in heterogeneous areas such as Tehran.

Table 7) Comparing the performance of GWR and OLR models.

Model	Dependent variable	Explanatory variable	Bandwidth	R^2	Adjusted R^2	Sigma	AIC
OLR	LST	NDVI	-	0.3	0.3	7.51	207370
GWR	LST	NDVI	166 m	0.93	0.89	1.07	137204

4- Conclusions

In this study, the relationship between the spatial- temporal changes of UHI and the green cover in Tehran was analyzed over a period of 24 years. First, the mono-window algorithm was applied to retrieve the LST of Tehran using the Landsat TM6 data. Then, the global and local spatial autocorrelation analyses were applied to quantify the characteristics of spatial and temporal changes of LST and NDVI at different scales and periods in Tehran. The exploration of spatial pattern in LST and NDVI images of Tehran clearly demonstrated the presence of significant spatial clusters of high and low values (hot and cold clusters) during the observed period 1987– 2010. We also found that the frequency and distribution of HH and LL clusters changed over time. The spatial pattern of the LST and UHI has expanded toward west and southwest of Tehran and the UHI effect was intensified. The LST trend showed an increase during study period while that of NDVI demonstrated a decreasing pattern. In contrast to hot spots, the green spots were accumulated over the north and east of Tehran. Based on the LISA analysis, the increasing trend of HH clusters of LST is closely related to the decrease of HH clusters of NDVI. Accompanying with decreasing of vegetation cover, green cover cooling effect also has decreased, and consequently, UHI effect was intensified from 1987 to 2010. Our results shows that most of the UHI controlled areas have been located in the western and southeastern parts of Tehran, where Mehrabad airport, commercial lands, the large industries, and barren lands are located. The distribution of LST shows largely significant difference between the west and southwest sectors and the north of city. These differences are related not only to the amount of vegetation, but also with the quality of the constructions. These land use types were covered by dark materials (such as asphalt, concrete, etc.) and metallic roofs (galvanized or aluminum materials) that have high absorbing power and store solar energy. The results demonstrate the usefulness of spatial autocorrelation technique for analysis of spatial and temporal changes of LST and green cover in urban areas. The relationship between LST and NDVI was investigated by the OLS and GWR models. Based on the diagnostic statistics, the GWR is stronger than the OLR model, and is characterized by the higher R2, lower AIC, and lower Sigma values. Due to spatial heterogeneity of Tehran urban area, the GWR model showed better performance in demonstrating the relationship between heat island intensity and vegetation cover than the OLS model.

Acknowledgments

The authors declare no conflict of interest.

References:

Akbari, H. 2000. Consideration of Temperature distribution pattern of Tehran using Landsat TM thermal data. Masters Dissertation, University of TarbiatModarres. Tehran, Iran.

Amiri, K., Weng, Q., Alimohamadi, A., Alavipanah, K. 2009. Spatial–temporal dynamics of land surface temperature in relation to fractional vegetation cover and landuse/cover in the Tabriz urban area, Iran. Remote Sensing of Environment: 113, 2606–2617.

Anselin, L. 1995. Local indicators of spatial association—LISA. Geogr Anal: 27, 93–115.

Balling, R. C., Brazell, S. W. 1988. High resolution surface temperature patterns in a complex urban terrain. Photogrammetric Engineering and remote sensing: 54, 1289–1293.

Bostan, P. A., Heuvelink, G. B. M., Akyurek, S. Z. 2012. Comparison of regression and kriging techniques for mapping the average annual precipitation of Turkey. International Journal of Applied Earth Observation and Geoinformation: 19, 115–126.

Chander, G., Markham, B. 2003. Revised Landsat-5 TM radiometric calibration procedures and post calibration dynamic ranges. IEEE Transactions on Geoscience and Remote Sensing: 41, 2674−2677.

Chen, Y., Shi, P., Li, X., He, C. 2002. Research on urban spatial thermal environment using remote sensing image. Acta Geodaeticaet Cartographica Sinica: 31, 322–326.

Cliff, A. D., Ord, J. K. 1981. Spatial Processes: Models and Applications. Pion, London.

Dai, X., Guo, Z., Zhang, L., Li, D. 2010. Spatio-temporal exploratory analysis of urban surface temperature field in Shanghai. China. Stochastic Environmental Research and Risk Assessment: 24, 247–257.

Du, M., Wang, Q., Cai, G. 2009. Temporal and spatial variation of urban heat island effect in Beijing using ASTER and TM. Urban Remote Sensing Joint Event, IEEE: 174–179.

Falahatkar, S.,Hosseini, S.M.,Soffianian, A.R. 2011. The relationship between land cover changes and spatial-temporal dynamics of land surface temperature. Indian Journal of Science and Technology: 4, 76–81.

Fotheringham, A.S., Brunsdon, C., Charlton, M. 2000. Geographically Weighted Regression: The Analysis of Spatially Varying Relationships. Wiley, Chichester, p.269.

Gallo, K.P., McNab, A.L., Karl, T.R., Brown, J.F., Hood, J.J.,Tarpley, J.D. 1993. The use of NOAA AVHRR data for assessment of the urban heat island effect. Journal of Applied Meteorology: 32(5), 899-908.

Gallo, K.P., Owen, T.W. 1998. Assessment of urban heat island: A multi-sensor perspective for the Dallas-Ft. Worth, USA region. Geocarto International: 13 (4), 35-41.

Gao, Y., Huang, J., Li, S., Li, S. 2012. Spatial pattern of non-stationary and scale-dependent relationships between NDVI and climatic factors: A case study in Qinghai-Tibet Plateau, China. Ecological Indicators: 20, 170–176.

Hallegatte, S., Henriet F., Corfee-Morlot, J. 2008. The Economics of Climate Change Impacts and Policy Benefits at City Scale: A Conceptual Framework, Environment Working No. 4, OECD, Paris.

Huo, X.N., Li, H., Sun, D.F., Zhou, L.D., Li, B.G. 2012. Combining Geostatistics with Moran's I Analysis for Mapping Soil Heavy Metals in Beijing, China. Int. J. Environ. Res. Public Health: 9, 995-1017.

Jangi, A. 2004. The role of location and morphology of city in the air quality of city by GIS and RS (the case study: Tehran). Masters Dissertation, University of Kharazmi, Tehran, Iran.

Legendre, P., Legendre, L. 1998. Numerical Ecology. Developments in Environmental Modelling. Elsevier, Amsterdam.

Li, J. 2006. Estimating land surface temperature from Landsat-5 TM. Remote Sens. Technol. Appl: 21, 322–326.

Li, J. J., Wang, X. R., Wang, X. J., Ma, W. C., Zhang, H. 2009. Remote sensing evaluation of urban heat island and its spatial pattern of the Shanghai metropolitan area, China. Ecological Complexity: 6, 413–420.

Li, S., Zhao, Z.,Miaomiao, X., Wang, T. 2010. Investigating spatial non-stationary and scale-dependent relationships between urban surface temperature and environmental factors using geographically weighted regression. Environmental Modelling and Software: 25, 1789–1800.

Liu, L., Zhang, Y. 2011. Urban heat island analysis using the Landsat TM data and ASTER data: a case study in Hong Kong. Remote Sensing: 3, 1535–1552.

Mo, X., Cheng, C.,Zhai, F., Li, H. 2011. Study on temporal and spatial variation of the urban heat island based on Landsat TM/ETM+ in

central city and Binhai New Area of Tianjin, Multimedia Technology (ICMT), 2011 International Conference on, 26-28 July 2011, 4616–4622.

Namdari, S. 2009. Extraction of urban heat island in urban regions by satellite images (the case study: Tehran). Master Dissertation. University of Shahid Beheshti, Tehran, Iran.

Qin, Z., Karnieli, A., Berliner, P. 2001. A mono-window algorithm for retrieving land surface temperature from Landsat TM data and its application to the Israel-Egypt border region. International Journal of Remote Sensing: 22, 3719–3746.

Rose, A. L., Devadas, M. D. 2009. Analysis of land surface temperature and landuse/land cover types using remote sensing imagery a case in chennal city, India. The seventh International Conference on Urban Climate, 29 June - 3 July 2009, Yokohama, Japan.

Ruth, M., Gasper, R. R. 2008. Water in the urban environment: Meeting the challenges of a changing climate. Proc. of OECD International Conference, OECD.

Streutker, D. R. 2002. A remote sensing study of the urban heat island of Houston, Texas. International Journal of Remote Sensing: 23, 2595–2608.

Sun, Q., Tan, J., Xu, Y. 2010. An ERDAS image processing method for retrieving LST and describing urban heat evolution: A case study in the Pearl River Delta Region in South China. Environmental Earth Sciences: 59, 1047–1055.

Su, W., Zhang, X., Wang, Z., Su, X., Huang, J., Yang, S., Liu, S. 2011. Analyzing disaster-forming environments and the spatial distribution of flood disasters and snow disasters that occurred in China from 1949 to 2000. Mathematical and Computer Modelling: 54, 1069–1078.

Van de Griend, A. A., Owe, M. 2003. On the relationship between thermal emissivity and the normalized difference vegetation index for natural surfaces. International Journal of Remote Sensing: 14, 1119–1131.

Voogt, J. A., 2002. Urban Heat Island. In Encyclopedia of Global Environmental Change, vol. 3: 660 - 666 (Chichester: Wiley.

Voogt, J. A.,Oke, T.R. 2003. Thermal remote sensing of urban climates. Remote Sensing of Environment: 86, 370–38.

Weng, Q. 2001. A remote sensing-GIS evaluation of urban expansion and its impact on surface temperature in the Zhujiang Delta, China. International Journal of Remote Sensing: 22, 1999–2014.

Weng, Q., Lu, D., Schubring, J. 2004. Estimation of land surface temperature–vegetation abundance relationship for urban heat island studies. Remote Sensing of Environment: 89: 467–483.

Weng, Q., Lu, D., Liang, B. 2006. Urban Surface Biophysical Descriptors and Land Surface Temperature Variations Photogrammetric Engineering and Remote Sensing: 72, 1275–1286.

Xu, H., Chen, B. 2004. Remote sensing of the urban heat island and its changes in Xiamen City of SE China. Journal of Environmental Sciences: 16, 276–281.

Xu, H., Chen, Y., Dan, S.,Qiu, W. 2011. Spatial and temporal analysis of urban heat island effect in Chengdu city by remote sensing. Geoinformatics, 19th international conference on, Shanghai, 24-26 June 2011, 1–5.

Zhang, J., Wang, Y., Li, Y. 2006. A C++ program for retrieving land surface temperature from the data of Landsat TM/ETM+ band6. Computers and Geosciences: 32, 1796–1805.

Zhang, J., Wang, Y., Wang, Z. 2007. Change analysis of land surface temperature based on robust statistics in the estuarine area or Pearl

River (China) from 1990 to 2000 by Landsat TM/ETM^{+} data. International Journal of Remote Sensing: 28, 2383–2390.